Deep-Sea Research I 105 (2015) 19–25

Contents lists available at ScienceDirect

Deep-Sea Research I

journal homepage: www.elsevier.com/locate/dsri

Ship motion effects in CTD-data from weakly stratified waters of the Puerto Rico trench

Hans van Haren *

Royal Netherlands Institute for Sea Research (NIOZ), P.O. Box 59, 1790 AB Den Burg, the Netherlands

ARTICLE INFO

Article history:
Received 8 April 2015
Received in revised form
24 June 2015
Accepted 12 August 2015
Available online 13 August 2015

Keywords:
Instabilities in weak stratification
Filter correction for ship motion
Direct pressure effect on conductivity
Direct velocity effect on temperature
Hadal zone
Puerto Rico Trench

ABSTRACT

Shipborne SBE 911plus Conductivity Temperature Depth (CTD)-casts have been made to maximum 7220 m in the Puerto Rico Trench (PRT). In PRT-waters from 5500 m and deeper and specifically below the 6500 m transition to the hadal-zone, the vertical density stratification is found very weak, with buoyancy frequency $N \approx 1.9$ cpd (cycles per day). In that zone, the nearly raw data are dominated by artificial oscillations of $\pm 5 \times 10^{-4}$ °C in temperature and of $\pm 5 \times 10^{-5}$ S m^{-1} in conductivity over ranges of 10 s ($\sim$10 m) intervals that are induced by the ship's heave of mean 2 m amplitude. The oscillations, only visible in very weak stratification, are different in *T* and *C* as they show: (1) a confirmation of the direct pressure effect on conductivity, assumed to be weak, and (2) an unknown effect of hoisting speed on temperature being negative for downcast and positive for upcast (and not affecting the *C*–*T* relationship). A low-pass filter is proposed to remove the artificial apparent overturns, whilst retaining the large-scale convection. This allows estimation of turbulence levels of the latter.

1. Introduction

A standard manner to establish the ocean's main state variables is using a shipborne Conductivity–Temperature–Depth (CTD) profiler, commonly mounted in a frame with additional sensors on, e.g., oxygen, transmission and fluorescence. The widely used instrument package is Sea-Bird Electronics SBE911plus CTD, with typical accuracies O(10^{-3}) °C for T and O(10^{-4}) S m^{-1} for C, resulting in about O(10^{-3}) g kg^{-1} for Absolute Salinity SA and O(10^{-3}) kg m^{-3} for density anomalies. Such high accuracy values are obtained after pre-deployment care, using well- and recently calibrated sensors, with T- and C-sensors mounted in a carefully vertically mounted pumped duct (Sea-Bird, 2012). Additionally, post-processing time-alignment of the sensors, conductivity's cell thermal mass correction and loop-edit correction for the ship's motion are needed. These procedures work well, although some problems around small-scale steps, mostly found in the upper ocean, are difficult to solve (e.g., Mensah et al., 2009).

However, specific problems may occur in very weakly stratified layers, where buoyancy frequency N=O(10^{-4} s^{-1}). A standard post-processed portion of downcast data from the deep Puerto Rico Trench demonstrates a regular spiking in all three main variables (Fig. 1a–c). Temperature is biased high, whilst salinity and density anomaly are biased low. This is observed in the weakly low-pass filtered (noise corrected), time-aligned and cell-thermal mass corrected profiles in purple, and in the same profiles after additionally using a standard loop-edit correction in blue. The spikes are only and correctly removed after employing a severe loop-edit correction of allowing a mere 20% variation in lowering (or hoisting) speed.

In this note, a more appropriate spike removal is suggested, including a better understanding of the effects of ship motion on *T*–*C* observations in weakly stratified waters. Apparently, these spikes are not removed by the use of a pumped TC-duct and much resemble, although with different interrelations, ship motion effects on un-pumped Neil Brown CTD-data from the well-stratified upper ocean (Trump, 1983). The aim is to obtain a reliable estimate of overturning scales (Fig. 1d) and associated turbulence parameter estimates (Thorpe, 1977) under such conditions.

2. Data

Observations have been made above Milwaukee Deep, the deepest part of the Puerto-Rico Trench from the Dutch R/V Pelagia. Using freshly calibrated *T*–*C* sensors, SBE911plus CTD-profiles were obtained at 19°44′N, 67°11′W in 8370 m water depth in December 2013 (one profile; another 100 km away). As per instructions from the manufacturer, the sensors were mounted vertically in a frame inside a 1.5 m high Rosette-Carousel holding 22 water sampling bottles. The CTD-frame was lowered via a heave compensator. During a second cruise two more profiles were obtained using the

* Corresponding author.
E-mail address: hans.van.haren@nioz.nl

http://dx.doi.org/10.1016/j.dsr.2015.08.002
0967-0637/

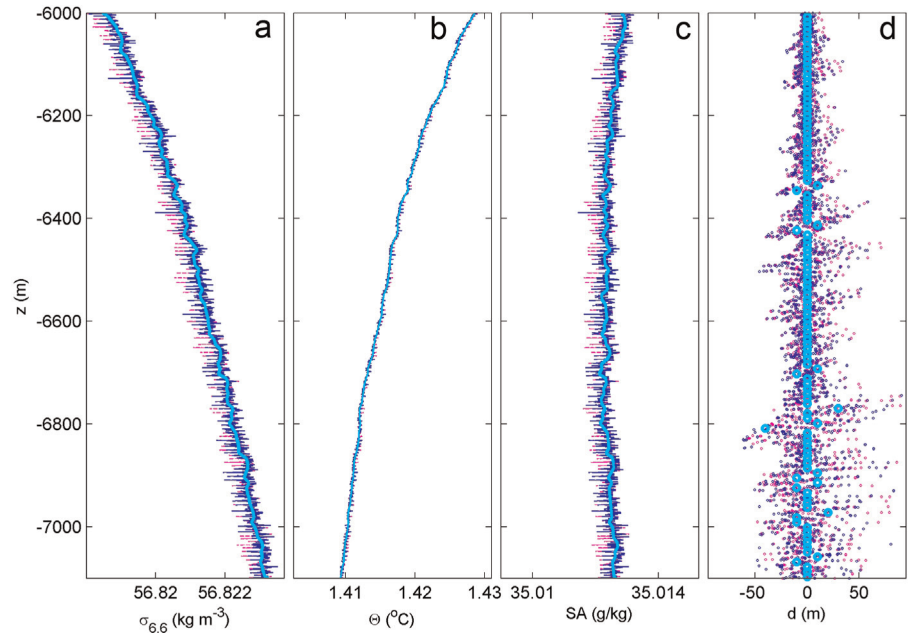

Fig. 1. Lower 1100 m detail of 2013 CTD-profile from the PRT. Standard processed (noise-filtered, time aligned and cell thermal mass corrected) "nearly-raw" data (purple) are compared with additionally weakly loop-edit corrected data (dark-blue; excluding velocities < 0.25 m s^{-1}) and heavily loop-edited data (light-blue; excluding velocities of 20% around the mean determined for a window of 300 s). (a) Potential density anomaly, referenced to the 6600 dbar. (b) Conservative Temperature. (c) Absolute Salinity. (d) Displacements of density inversions with respect to their reordered statically stable density-anomaly profile.

same CTD but a different winch without heave compensator and without the Rosette-Carousel at the above position in February 2015. A maximum profiling depth of 7220 m was due to pressure sensor and cable length constraints.

The CTD is used in a standard configuration, with T- and C-sensors vertically mounted in a "TC-duct" attached to a 3000 rpm pump, realizing a flow speed of 2.3 m s^{-1}. The sensors are near the bottom of the electronics frame, with a nearly unobstructed flow exposure, except for a thin crossbar, when moving downward. The exhaust of the pumped duct is at the same (pressure) level as the intake, so as to eliminate the ram effect of dynamic pressure (Sea-Bird, 2012). Thus, in theory the flow speed is constant past the sensors, which simplifies the dynamic response calibration (Gregg and Hess, 1985) by eliminating errors in T-measurement due to sensor-friction ($\approx +1\times10^{-3}$ °C for a 1 m s^{-1} flow speed; Larson and Pedersen, 1996) and weaker errors due to flow-induced pressure variations in an adiabatic lapse rate environment ($p_d = 1/2\rho U^2$, ρ the water density; for a speed range of $U = [0, 4.5]$ m s^{-1} this yields a pressure range of [0, 1] dbar).

The raw CTD-data are processed using the standard procedures incorporated in SBE-software, including corrections for cell thermal mass, time-alignment and some modest low-pass filtering. Temperature sensor data are transferred to Conservative ($\sim$potential) Temperature (Θ) values (IOC, SCOR, IAPSO, 2010).

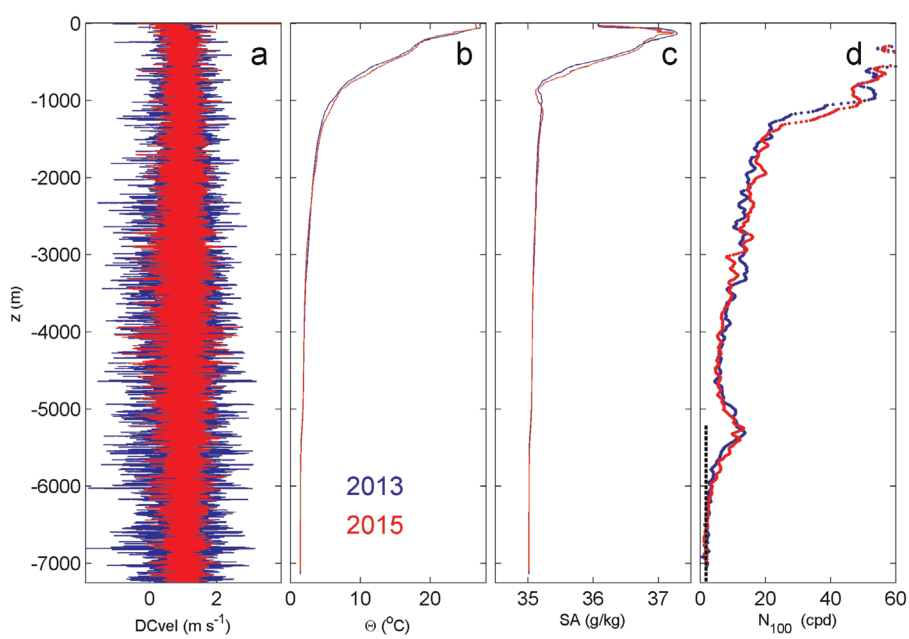

Fig. 2. Full depth overview of 1 m vertically binned CTD-data observed in December 2013 (blue) and February 2015 (red) in the PRT. (a) Downcast velocity, computed from the first derivative of pressure. (b) Conservative Temperature. (c) Absolute Salinity. (d) Buoyancy frequency, smoothed over 100 m vertical scales. The vertical dashed line is at $N = 2$ cycles per day. (For interpretation of the references to color in this figure legend, the reader is referred to the web version of this article.)

Density anomalies $\sigma_{6.6}$ are referenced to 6600 dbar. Under particular assumptions the data are tested to be used to estimate turbulence parameters dissipation rate ε and vertical eddy diffusivity K_z using the method of reordering potentially unstable vertical density profiles in statically stable ones, as proposed by Thorpe (1977).

3. Observations

The deep CTD-casts, made 14 months apart, returned very similar data (Fig. 2). Conservative Temperature (Fig. 2b) and Absolute Salinity (Fig. 2c) both decrease with depth below 1000 m, but temperature decreases faster so that it dominates the stable density stratification (Fig. 2d). Relatively large stratification $N > 10$ cpd (cycles per day) is observed between about 5000 and 5500 m, the depth range corresponding to the sea floor depth of the abyssal plain to the north of PRT. The main difference between the presented 2013 and 2015 data, and between the two other profiles taken within a day, is the depth of > 100 m scale variations that reflect the vertical excursion of dominant internal waves.

At depths greater than 6000 m, the stratification is very weak, but still significantly different from zero as $N = 2 \pm 0.7$ cpd (dashed vertical line in Fig. 2d). In the depth range [6000, 7200] m, all main variables show a dominant oscillation with time having relatively short periods from 8 to 10 s (Figs. 3 and 4). For pressure p this is a continuation from what can be observed throughout the entire profile (Fig. 2a) and which is associated with ship's motion due to surface waves. Although sea conditions were more favorable in 2015 (2–3 m surface waves; 10–12 m s^{-1} wind speeds) than in 2013 (3–4 m; 12–14 m s^{-1}), it is seen that beyond the range of the heave-compensator (upper 1500 m in the 2013 profile), the effects of ship motion are evenly communicated through the profile, with a slight damping in the lower 1000 m. A better heave-compensator used by Taira et al. (2005) can eliminate about 75% of the ship motions at great depths. As their aim was to study large-scale water mass variations, we cannot establish effects as presented here on the remaining influence of ship motions in their data.

For temperature (Fig. 3b) and conductivity (Fig. 3c), these

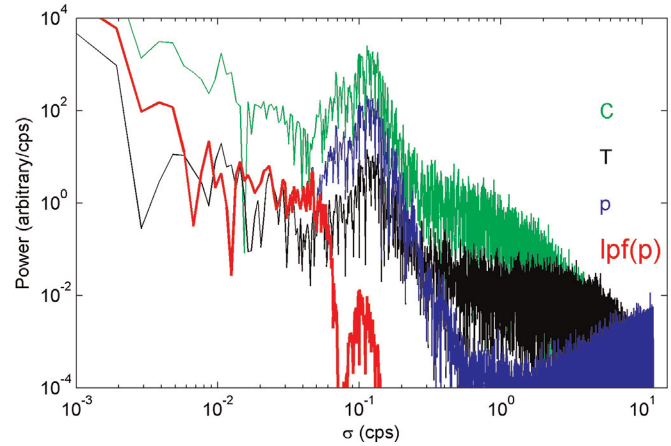

Fig. 4. Nearly unsmoothed (~3 degrees of freedom) spectra of nearly raw 24 Hz sampled CTD-data from the 6000–7000 m depth range. The red spectrum is the < 0.05 cps low-pass filtered version of the blue p-spectrum. (For interpretation of the references to color in this figure legend, the reader is referred to the web version of this article.)

short-period oscillations can only be observed in weak stratification, when the local adiabatic lapse rate (here around 6650 dbar $\Delta T/\Delta p = \Gamma_T \approx 1.5 \times 10^{-4}$ °C dbar^{-1}) dominates the vertical temperature gradient ($dT/dz \approx -1.3 \times 10^{-4}$ °C m^{-1}). This small difference in (absolute) slope does warrant a measurable and significantly different from zero stratification (*cf.*, van Haren and Millot, 2006, also for truly homogeneous profiles). Whilst conductivity oscillations (Fig. 3c), relative to the large-scale variations (local "mean"), appear in phase with relative pressure oscillations (Fig. 3a), the relative temperature oscillations (Fig. 3b) are found π out-of-phase with the time derivative of both p and C. This gives the following observed relationships, for the short section of example data in Fig. 3

$$\Delta C = \gamma_C \Delta p, \quad \gamma_C = 3 \pm 0.5 \times 10^{-5}\ \mathrm{S\ m^{-1}\ dbar^{-1}}, \tag{1}$$

$$\Delta T = \gamma_T\, dp/dt, \quad \gamma_T = -3 \pm 1 \times 10^{-4}\ ^\circ\mathrm{C\ s\ dbar^{-1}}. \tag{2}$$

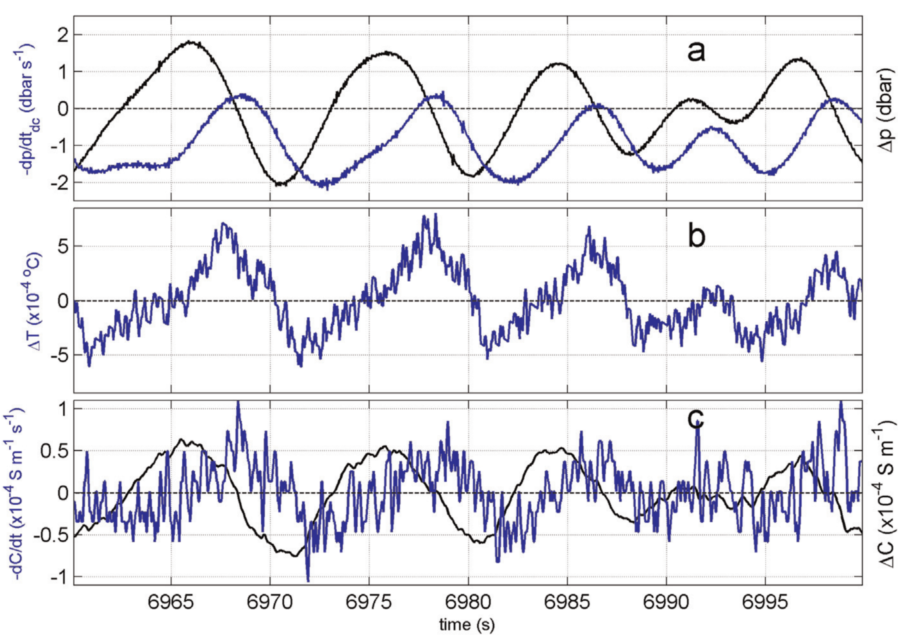

Fig. 3. Short example time series of nearly raw 2013 data for the vertical range $-6543 < z < -6506$ m. (a) Detrended pressure (black) and its (negative signed) first time derivative (blue). (b) Detrended temperature. (c) Detrended conductivity (black) and its (negative signed) first time derivative (blue). (For interpretation of the references to color in this figure legend, the reader is referred to the web version of this article.)

Combining (1) and (2) it is inferred that

$$\Delta T = \gamma_2 dC/dt, \quad \gamma_2 = -10 \pm 2\ ^\circ\mathrm{C\ s\ m\ S^{-1}}, \tag{3}$$

as observed (Fig. 3b and c).

To within error, the γ_C in (1) matches value and sign of the known "weak" pressure dependence of conductivity cells. Following Horne and Frysinger (1963) and algorithms (tables) in Fofonoff and Millard (1983) the established computed dependence is $\Delta C \approx 2.6 \times 10^{-5} \Delta p$ (S m^{-1} dbar^{-1}) for T=0 °C, practical salinity S=35 psu and p=6000–7000 dbar. The observed relationship (1) thus confirms, and in fact measures, the direct effect of pressure oscillations on conductivity.

For temperature oscillations however, such a direct pressure effect is not observed. As is visible in Fig. 3, T-oscillations are delayed by about $\pi/2$ with respect to p (and C). They thus correspond best with the uneven time derivatives of p and C, as in (2) and (3). As will be elaborated in Section 4, this implies a temperature-correspondence with velocity, instead of pressure, oscillations. A direct effect of pressure oscillations of amplitude $|\Delta p|$=1.5 dbar would result in an adiabatic expansion temperature change of $\pm 2.2 \times 10^{-4}$ °C, which is more than a factor of 2 lower than the observed $\Delta T \approx 5 \times 10^{-4}$ °C (Fig. 3b). In Fig. 3, no adiabatic influence is noticeable; the observed variations in conductivity are a factor of 4 lower than those attributable to the observed temperature oscillations, given the common C–T relationship (Fofonoff and Millard, 1983). This difference in values of γ_T and Γ_T by a factor of 2 adds to their signs being opposite: lower/higher temperature is observed with higher/lower downward velocities during CTD's downcast, with a notable sudden increase in temperature when the speed approaches zero (from decreasing downward speed).

The absolute value of $|\gamma_2|$ found in (3) is close to the typical temperature–dependence of conductivity, $\Delta T/\Delta C$=12 °C m S^{-1} for practical salinity S=35 psu, p=6000 dbar and a temperature range of [0, 10] °C (Fofonoff and Millard, 1983). Here too however, the direct temperature effect is not noticeable in conductivity, due to the $\pi/2$ phase difference.

The ship's motions communicated to the CTD-package occupy a moderately broad frequency range around σ=0.11 cps (cycle per second), so typical for a surface wave spectrum (Fig. 4). At depths shallower than 6000 m, in stratification with $N >> 2$ cpd, the natural (internal wave) variations in C and T cause spectra to increase their levels above those in Fig. 4, so that surface wave peaks merge with the spectral background. Here, for the depth range of 6000–7000 m and $N \approx 2$ cpd, the spectra of T and C roll-off from level white noise, due to the low-pass filter ("SBE-lpf") applied for $\sigma > 3$ cps (on T) and > 0.7 cps (on C) using the SBE-post-processing software. To remove the surface wave effect (equally in all three main variables), application of a band-pass filter on the original time series would be sufficient. However, as at least T and C are basically white noise for $\sigma > 0.3$ cps, only a sharp double elliptic filter passing frequencies below $\sigma < 0.05$ cps (red graph in Fig. 4) retains meaningful data. The filter-form is a modified Kaiser-window (Parks and Burrus, 1987) and is named here "NIOZ-lpf", to distinguish it from the above SBE-lpf with higher frequency cut-offs. It is noted that the NIOZ-lpf is a low-pass filter applied on time series, not on pressure series. Thus, it correctly accommodates for variations in CTD's motion (velocity), which are aliased over a broad band in pressure series.

The NIOZ-lpf filtered data (Fig. 5) demonstrate that in the hadal zone (below 6500 m) the large-scale density stratification (Fig. 5a) is dominated by Conservative Temperature stratification (Fig. 5b) with weaker (or negative) contributions from Absolute Salinity (Fig. 5c). As in Fig. 2, the three panels a–c in Fig. 5 have the same x-axis range in terms of density change.

Although sea conditions were better in February 2015, yielding less extensive pressure oscillations (Fig. 2a), the filtered data in Fig. 5 are remarkably similar between 2013 and 2015, with the exception of a 0.0013 g/kg shift in Absolute Salinity, independent of depth (in the presented range). This shift is within the limitation of accuracy of salinity estimation, due to variations from batch to batch in standard seawater of 0.002 PSU (Mantyla, 1987). On shorter vertical scales, the two profiles vary, as do the other two obtained additionally during both cruises. In salinity (and density), these short-scale variations are attributable in part to noise extended to about 0.02 cps.

This increased noise range in C-, and thus in SA- and $\sigma_{6.6}$-variations implies that the latter can still not be used without a certain enhanced threshold to estimate turbulence parameters (e.g., Stansfield et al., 2001). Applying a threshold of 5×10^{-5} kg m^{-3} for density differences (commensurate the

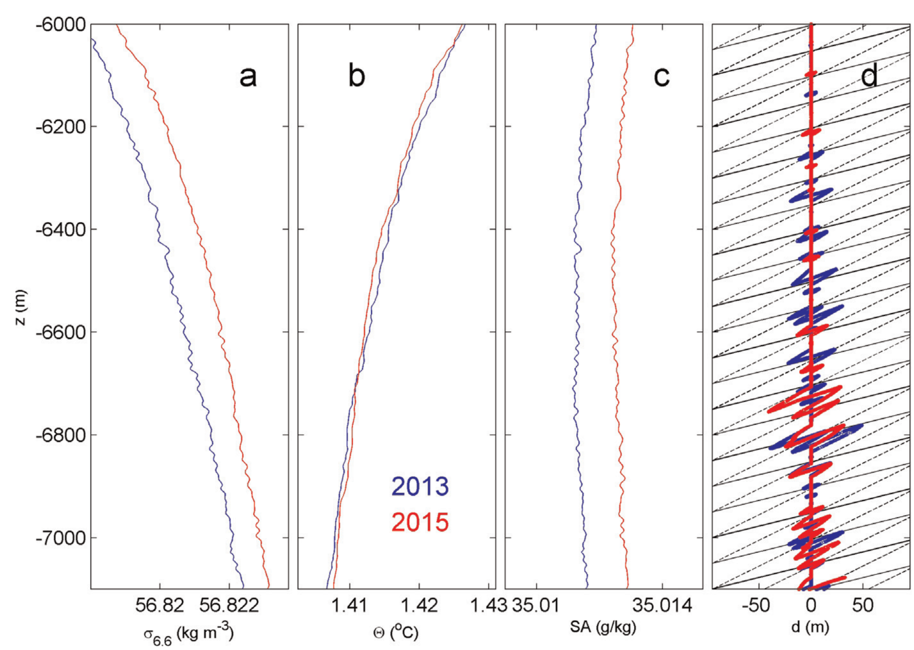

Fig. 5. As Fig. 1, but for < 0.05 cps low-pass filtered data and including a similarly filtered 2015 profile. (Panel d) slopes ½ (solid lines) and 1 (dashed lines) are indicated.

Table 1
Mean turbulence parameter estimates from differently processed CTD-data between 6400 and 7000 m in the PRT, using the reordering method of Thorpe (1977). The buoyancy frequency is locally determined from the reordered profile; for the turbulence parameters a constant mixing efficiency of 0.2 and a constant ratio of 0.8 between overturning and Ozmidov scales are used. Unless indicated, all estimates are using Conservative Temperature downcast profiles only in combination with a fixed linear temperature–density relationship, established for the same range using the CTD-data.

	Data processing type	N (s^{-1})	ε ($\mathrm{m}^2\,\mathrm{s}^{-3}$)	K_z ($\mathrm{m}^2\,\mathrm{s}^{-1}$)
I	SBE: weak low-pass filter, time-align, cell thermal mass; no loop-edit (Fig. 1, purple)	1.7×10^{-4}	1.1×10^{-8}	7.2×10^{-3}
II	As I, and >0.25 m s^{-1} loop-edit (Fig.1, blue)	1.7×10^{-4}	1.0×10^{-8}	6.8×10^{-3}
III	As I, and 300 s window, >0.5 m s^{-1}, 20% loop-edit (Fig. 1, light-blue)	1.7×10^{-4}	1.2×10^{-10}	1.0×10^{-3}
IV	As I, and <0.05 cps low-pass filter (Fig. 6)	1.7×10^{-4}	4.8×10^{-11}	9.8×10^{-4}
V	As I, and <0.05 cps lpf; $\sigma_{6.6}$ ($>5\times10^{-5}$ kg m^{-3})	1.8×10^{-4}	6.7×10^{-11}	5.3×10^{-4}
VI	As I, and <0.05 cps lpf Upcast	1.6×10^{-4}	5.6×10^{-11}	1.2×10^{-3}

0.05 cps NIOZ-lpf filtering and hence a 20-fold reduction of standard noise of about 10^{-3} kg m^{-3}) between original and reordered statically stable profiles, yields overturn values that are comparable to within a factor of 2 with those established using Conservative Temperature and a linear Θ–$\sigma_{6.6}$-relationship (Fig. 5d). The 6400–7000 m average turbulence parameter values of the filtered data are one (K_z) and two (ε) orders of magnitude smaller than those estimated using the original, weakly post-processed data (Table 1). They are also smaller (by a factor of 2 in ε) than the heavily loop-edited data.

Although the improved estimate values seem low ($\varepsilon < 10^{-10}\,\mathrm{m}^2\,\mathrm{s}^{-3}$), the typical overturn sizes of d=20–50 m correspond well with convection cells observed in the weakly stratified deep Mediterranean (van Haren and Gostiaux, 2011). There, they were induced by 150 m large inertial waves; here they are more likely induced by internal tides of possibly equal amplitude. Such large internal waves in the weakly stratified deep-sea well away from surface and bottom boundaries are understood, because of the weak restoring force of reduced gravity (or momentum for gyroscopic waves). The shapes and slopes of the overturns mainly resemble, in a clear fashion unperturbed by instrumental noise, half-turn Rankine vortices (a single zig-zag with central slope slightly exceeding ½ (z/d) and side-slopes slightly exceeding 1 (z/d); van Haren and Gostiaux, 2014) and occasionally a full-turn Rankine vortex (double zig-zag, e.g., around 6600 and 6800 m in the blue profile, Fig. 5d). The observations suggest Rankine vortices representing shear-convective turbulence to be an adequate model for observed overturning, also in the present predominantly free convective, weakly stratified waters. Further details await future analysis of moored high-resolution temperature sensor data.

4. Discussion

The down- and upward motion at an approximate 1 m s^{-1} speed of a CTD instrument package, commonly attached in a Rosette-frame with additional sensors and water sampling bottles thus exceeding a volume of $>1\,\mathrm{m}^3$, yields a Reynolds number Re $\sim10^6$. It thus generates fully developed turbulence. The form drag around the obstacles of frame and instruments including the cylindrical CTD-sensors causes a quasi-laminar bulb of fluid being pushed in front, with detachment along the sides and a turbulent mixing wake with possible meandering dragged along behind them. Variations in speed do not much alter the turbulence state, as Re will always be high, but may imply different turbulence states of water sampled. When moving downward, the front bulb will cause additional pressure at the entrance of the TC-duct leading to the T- and C-sensors. When moving upward, the turbulent rear-wake lowers the pressure at the TC-duct entrance. It is speculated that this change in pressure at the TC-duct entrance modifies the flow rate through the duct, but in an unconventional way.

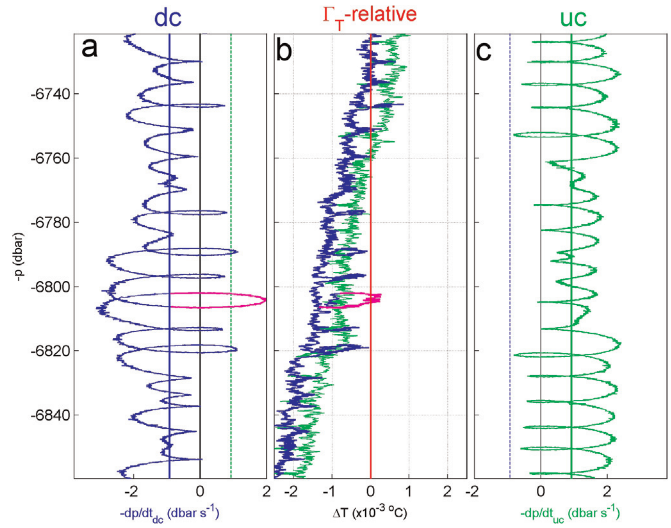

Fig. 6. Temperature variations as a function of velocity during downcast (dc; blue) and upcast (uc; green) for a 120 dbar range around 6800 dbar. (a) Negative time derivative of pressure, ∝vertical velocity, during downcast. The purple portion is a large loop with velocities above the average for the depicted range (vertical blue line; -0.94 dbar s^{-1}). The dashed green line indicates the mean velocity for the upcast. (b) Observed temperature relative to the local adiabatic lapse rate. The purple loop corresponds to the one in the pressure data. (c) As (a), but for upcast data. (For interpretation of the references to color in this figure legend, the reader is referred to the web version of this article.)

Not only 10 s oscillations, but also quasi-steady differences of about 0.6×10^{-3} °C are observed in temperature, between down- and upcast profiles (Fig. 6b), T-upcast being consistently higher than T-downcast. Such a difference, with the same sign, has also been observed using an Ifremer SBE911plus CTD mounted in a different frame and lowered from a different ship in truly homogeneous waters (so that temperature strictly followed the local adiabatic lapse rate) in the deep Western Mediterranean, under calm sea state conditions (van Haren and Millot, 2006). Elaborating here, the $\pm3\times10^{-4}$ °C temperature difference between up- and downcast is related with the ±0.93 m s^{-1} velocity difference, where upward velocity W is here taken as positive. Thus, as $-\mathrm{d}p/\mathrm{d}t \propto +W$, the ∝-sign incorporating the transfer from db- to m-units, the observed steady temperature difference fits well the relationship (2) found for the short-period oscillations.

Thus during downcast, measured T is on average too cool, by -3×10^{-4} °C. When the speed becomes less than average or velocities even change sign as in the purple trajectory in Fig. 6a, temperature reacts immediately and increases, first to its “correct” value (at the mean downcast speed), and subsequently to higher values, reaching T-upcast at about 0 speed. In the depicted case, the retro-up moving CTD exceeds the T-upcast (green) value when the upward speed is higher than the upcast (green) average (dashed line in Fig. 6a). After retrograding 1.5 m or the height of the CTD-frame, the sensors sample the fully turbulent, low pressure wake dragged down behind the CTD-package before, as the observed temperature now follows the adiabatic lapse rate (red line in Fig. 6b). Even after correcting the temperature increase by

-3×10^{-4} °C to “adjust” the $2\,\mathrm{m\,s^{-1}}$ upward speed to the mean upcast speed, the retro-up (from downcast) temperature exceeds the common (green) upcast temperature by some $+6\times10^{-4}$ °C. Hypothetically, this is the temperature increase due to homogenization, or water dragged adiabatically from about 60 m higher-up. The reversal of the purple loop shows some hysteresis, as the CTD does not return at the previous T-downcast trace until in new waters, i.e., when outside the CTD's turbulent wake and at pressures beyond the highest before the loop. Note that the turbulent wake T-difference of about 1.1×10^{-3} °C between retro-up and back-downcast-again is commensurate the difference in (enhanced) speeds, as in (2).

More or less the reverse is observed for loops in the upcast profile. Note that this profile, which is generally thought to represent measurements sampled in turbulent (mixing) waters, does not follow the local adiabatic lapse rate, but retains the slope of weak stratification as for the downcast. Apparently, the large-scale convection pattern is not disturbed by the (turbulent) motion of the CTD-package, or only unmeasurable locally.

The proposed solution to eliminate the erroneous oscillatory data due to ship's motion is a low-pass filtering of time series. It is not possible to apply such NIOZ-lpf filter on (binned) pressure series: in a wave-number spectrum the pressure loops give a broadband smearing of the peaks appearing in the frequency spectrum (Fig. 4). The applied filter, apt for the local surface wave effects, retains variations with periods >20 s, or approximately >19 m in vertical scale height. This resolves the larger scale overturns, so typical for Rayleigh–Taylor free turbulence convection, which probably is in a slantwise direction in the weakly stratified waters of the deep PRT. Around 4000 m in the Eastern Mediterranean, such convection has been observed to exhibit vertical scales of 50–150 m, as far as could be established using a 100 m limited string of high-resolution temperature sensors (van Haren and Gostiaux, 2011).

The present CTD-profiles were obtained in open ocean waters, using the mid-ship A-frame of a medium size (67 m long) ocean-going research vessel under moderately strong wind and swell conditions. The observed T- and C-oscillations are thus likely to occur more commonly and not only in deep trenches. Although they are small and detected in weakly stratified waters in the deep ocean, the ship's motion is communicated to the CTD-package throughout the entire vertical profile, even when a partial heave-compensator is used, as is visible in the pressure data. The pressure inversions (“loops”) thus affect near-surface waters as well. They should be visible in near-homogeneous step-like layers when such are larger than 10 m in height, as for example found in the Western Atlantic and in the Mediterranean. In the present profiles they create a non-significant, barely visible dent in the flat-slope of T- and C-spectra. They are thus different from previous not-pumped CTD-systems (Trump, 1983). The T- and C-oscillations in the latter historic observations were dependent on the stratification rate, and showed identical dependence of T- and C on the hoisting, albeit with highly variable, between 0 and π phase difference at different depths. Thus, Trump's (1983) relationships cannot explain the present observations.

If present, such near-surface oscillations could be removed using the proposed NIOZ-lpf. However, this filter will also remove the O(1 m) thin, strongly stratified layers above and below such near-homogeneous layers. It should be investigated how much harm is done by such removal on, e.g., estimates of overturning scales in the upper ocean, as such estimates are presently biased by artificial effects of sensor-mismatch over thin layers, generally causing a salinity/density spike, and which is difficult to resolve completely by tuning cell thermal mass parameters (cf., Mensah et al., 2009).

The observed increase of deep-T, when sampled in presumably lower (wake) pressure, is contrary to general thermodynamics (that are related with sensor friction; the dynamic pressure ram effect) and it is not prevented by the TC-duct. Although the erroneous data could be isolated and a proper correction be applied, the precise cause for the counter-intuitive temperature–velocity relationship needs to be established yet. The 1.5 m high frame moving in about adiabatic lapse rate temperature gradients is not providing the heat release after thermal mass storage that explains the observed sudden temperature increase at 0-speed, for example. The same 0-speed *T*-increase can also not be explained from the heating of the CTD's electronics at a rate of about 1.2×10^{-4} °C $\mathrm{L^{-1}\,s^{-1}}$ and which yields an asymmetric, because upward-moving convective response in the weakly stratified waters.

The observations may be explained by flow-induced pressure variations at the TC-duct yielding overpressure during downward motion thereby counteracting the pump-flow (and the reverse during upward motion). This needs to be verified by measuring flow in the TC-duct of a moving CTD. Meanwhile, as a precaution, one could experiment by mounting the CTD-sensors pump tubing horizontally, preferably sticking out of the frame. The latter however, makes CTD-retrieval a difficult task. For the present data, the proposed low-pass filter seems adequate as overturns at vertical scales <20 m are not expected to contribute significantly to the turbulence parameter estimates in weakly stratified deep-sea waters.

5. Conclusions

The following can be concluded from the present analysis using shipborne CTD-data in weakly stratified waters:

- Ship motion effects are detected in data of the primary variables conductivity and temperature.
- A direct effect is observed of pressure on conductivity variations.
- A direct effect is observed of hoisting velocity, i.e., pressure time derivative, on temperature variations.
- Given the above observations, a most likely cause of the ship motion effects are unwanted flow-induced pressure variations in the pumped TC-duct.
- As a remedy, a low-pass filter is proposed to be used on time series of the primary variable, before estimating turbulence parameters using the method of reordering to statically stable (density) profiles.

Acknowledgments

Captain and crew of the R/V Pelagia are thanked for the pleasant cooperation during the sea operations. I thank N. Larson (SBE) for stimulating advice.

References

Fofonoff, N.P., Millard, R.C., 1983. Algorithms for Computation of Fundamental Properties of Seawater. UNESCO, Paris, France, pp. 1–53 (UNESCO Technical Papers in Marine Science 44).

Gregg, M.C., Hess, W.C., 1985. Dynamic response calibration of Sea-Bird temperature and conductivity probes. J. Atmos. Ocean. Technol. 2, 304–313.

Horne, R.A., Frysinger, G.R., 1963. The effect of pressure on the electrical conductivity of sea water. J. Geophys. Res. 68, 1967–1973.

IOC, SCOR, IAPSO, 2010. The International Thermodynamic Equation of Seawater – 2010: Calculation and Use of Thermodynamic Properties. Intergovernmental Oceanographic Commission, Manuals and Guides No. 56, UNESCO, Paris, France, pp. 1–196.

Larson, N., Pedersen, A.M., 1996. Temperature measurements in flowing water: viscous heating of sensor tips. In: Proceedings of the 1st IGHEM Meeting.

Montreal, PQ, Canada. Available online at: ⟨http://www.seabird.com/technical_references/viscous.htm⟩.
Mantyla, A.W., 1987. Standard seawater comparisons updated. J. Phys. Oceanogr. 17, 543–548.
Mensah, V., Le Menn, M., Morel, Y., 2009. Thermal mass correction for the evaluation of salinity. J. Atmos. Ocean. Technol. 26, 665–672.
Parks, T.W., Burrus, C.S., 1987. Digital Filter Design. Wiley, New York, USA, pp. 1–342.
Sea-Bird, 2012. Fundamentals of the TC duct and pump-controlled flow used on Sea-Bird CTDs. Proceedings of the Sea-Bird Electronics Application Note 38, SBE. Bellevue, WA, USA, p. 1-5.
Stansfield, K., Garrett, C., Dewey, R., 2001. The probability distribution of the Thorpe displacement within overturns in Juan de Fuca Strait. J. Phys. Oceanogr. 31, 3421–3434.
Taira, K., Yanagimoto, D., Kitagawa, S., 2005. Deep CTD casts in the Challenger Deep. Mariana Trench. J. Oceanogr. 61, 447–454.
Thorpe, S.A., 1977. Turbulence and mixing in a Scottish loch. Philos. Trans. R. Soc. Lond. A 286, 125–181.
Trump, C.L., 1983. Effects of ship's roll on the quality of precision CTD data. Deep-Sea Res. 30, 1173–1183.
van Haren, H., Gostiaux, L., 2011. Large internal waves advection in very weakly stratified deep Mediterranean waters. Geophys. Res. Lett. 38, L22603. http://dx.doi.org/10.1029/ 2011GL049707.
van Haren, H., Gostiaux, L., 2014. Characterizing turbulent overturns in CTD-data. Dyn. Atmos. Oceans 66, 58–76.
van Haren, H., Millot, C., 2006. Determination of buoyancy frequency in weakly stable waters. J. Geophys. Res. 111, C03014. http://dx.doi.org/10.1029/2005JC003065.